

Supporting Information

Strongly Coupled 3D Ternary Fe₂O₃@Ni₂P/Ni(PO₃)₂ Hybrid for Enhanced Electrocatalytic Oxygen Evolution at Ultra-high Current Densities

Xiaodi Cheng^a, Zhiyan Pan^b, Chaojun Lei^a, Yangjun Jin^b, Bin Yang^a, Zhongjian Li^a,
Xingwang Zhang^a, Lecheng Lei^a, Chris Yuan,^c Yang Hou^{a,*}

^aKey Laboratory of Biomass Chemical Engineering of Ministry of Education,
College of Chemical and Biological Engineering, Zhejiang University, Hangzhou,
China

^bEnvironmental Chemical and Resource Research Institute, College of
Environment, Zhejiang University of Technology, Hangzhou, China

^cDepartment of Mechanical and Aerospace Engineering, Case Western Reserve
University, Cleveland, OH, 44106, USA

* E-mail: yhou@zju.edu.cn;

Experimental section

Preparation of Ni₂P/NF.

Commercial Ni foam was washed in an ultrasonic machine with acetone, hydrochloric acid, ethanol, and deionized water for 10 min, respectively. After above treatments, three pieces of Ni foams were thermally phosphorization at 300 °C for 1 h with 100 mg of red phosphorus in a vacuum quartz tube.

Preparation of Fe₂O₃@Ni₂P/Ni(NO₃)₂/NF.

Commercial Ni foam was washed in an ultrasonic machine with acetone, hydrochloric acid, ethanol, and deionized water for 10 min, respectively. After above treatments, three pieces of Ni foams were dipped into an 0.15 M of Fe(NO₃)₃ and dried in fume hood at room temperature, and then thermally phosphorization at 300 °C for 1 h with 100 mg of red phosphorus in a vacuum quartz tube. The loading amount of Fe@Ni₂P/Ni(PO₃)₂ catalyst was ~1.2 mg cm⁻².

Preparation of Fe₂O₃/NF.

Commercial Ni foam was washed in an ultrasonic machine with acetone, hydrochloric acid, ethanol, and deionized water for 10 min, respectively. After above treatments, three pieces of Ni foams were dipped into 0.15 M of Fe(NO₃)₃ solution and dried in fume hood at room temperature, and then thermally treated at 300 °C for 1 h in a vacuum quartz tube.

Preparation of Ir/C/NF.

The mixture of 8 mg of Ir/C, 900 μL of Nafion (5%), and 100 μL of ethanol was ultrasonicated for 30 min, and then oscillated with oscillator obtain a uniform

dispersion. After the Ir/C dispersal was dipped onto the above treated Ni foam, the Ir/C/NF taster was gradually dried in fume hood. The loading amount of Ir/C catalyst was $\sim 1.2 \text{ mg cm}^{-2}$.

Preparation of Pt/C/NF.

The mixture of 8 mg of Pt/C, 900 μL of Nafion (5%), and 100 μL of ethanol was ultrasonicated for 30 min, and then oscillated with oscillator obtain a uniform dispersion. After the Pt/C dispersal was dipped onto the above treated Ni foam, the Pt/C/NF taster was gradually dried in fume hood. The loading amount of Pt/C catalyst was $\sim 1.2 \text{ mg cm}^{-2}$.

Characterization.

The morphology of samples was measured with Supra 55 field-emission scanning electron microscope (FESEM). The high-resolution TEM images of samples were attained using JEM-2100 high-resolution transmission electron microscopy (200 kV). X-ray diffraction (XRD) patterns were evaluated on the RIGAKU D/MAX 2550/PC X-ray diffractometer using Cu $K\alpha$ radiation. Raman tests were measured on a LabRAM HR Evolution Laser Confocal Raman Microspectroscopy with the wavelength of 532 nm. X-ray photoelectron spectroscopy (XPS) spectra were operated on Escalab 250Xi X-ray photoelectron spectroscopy using Al $K\alpha$ radiation. All XPS spectra results were calculated after correction with C 1s peak at 284.8 eV.

Electrochemical measurements

The electrochemical test was measured in a three-electrode cell using 1.0 M KOH as the electrolyte. A Pt sheet (1 cm \times 1 cm) was used as the counter electrode, and

Ag/AgCl electrode was used as reference electrode. The Ir/C/NF, Fe₂O₃/NF, Ni₂P/NF, and Fe₂O₃@Ni₂P/Ni(NO₃)₂/NF were analyzed as working electrodes directly. Before the measurements of electrochemical properties, these catalysts were activated with numerous cyclic voltammetry cycles until they were stable. The OER catalytic activity was gained by using linear sweep voltammetry with a scan rate of 5 mV s⁻¹. The Tafel slope was calculated from the above linear sweep voltammetry curve. The mechanical robustness and stability was studied through multiple-current steps, multiple-potential steps, and amperometric current-time assessment. Electrochemical impedance spectroscopy was measured at potential of 1.55 V with frequency from 0.01 Hz to 10⁵ Hz. All of these measured potentials vs. Ag/AgCl electrode which were switched to the potentials vs. RHE using the Nernst equation: $E_{\text{RHE}} = E_{\text{Ag/AgCl}} + 0.0591 \text{ pH} + 0.098 \text{ V}$.

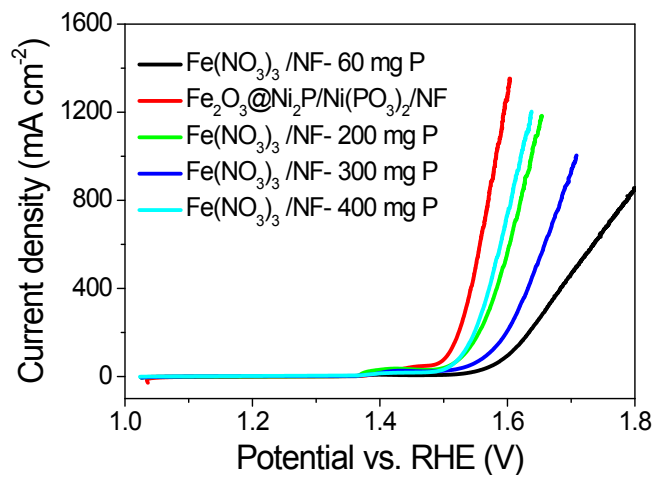


Figure S1. Polarization curves of Fe₂O₃@Ni₂P/Ni(NO₃)₂/NF hybrid with different amount of red phosphorus.

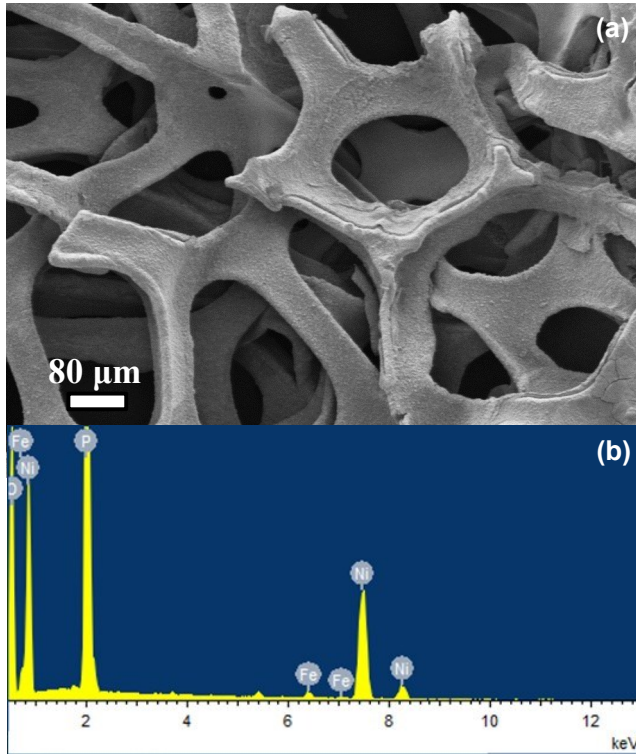


Figure S2. (a) FESEM image of NF, (b) EDX spectrum of $\text{Fe}_2\text{O}_3@\text{Ni}_2\text{P}/\text{Ni}(\text{NO}_3)_2/\text{NF}$.

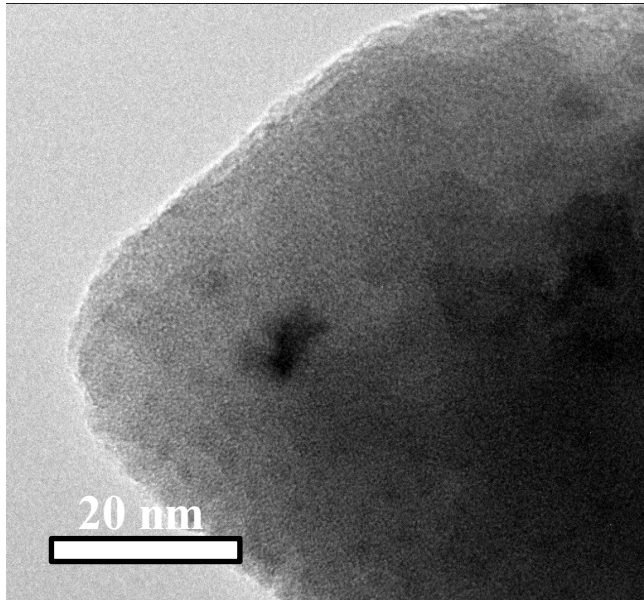


Figure S3. TEM image of $\text{Fe}_2\text{O}_3@\text{Ni}_2\text{P}/\text{Ni}(\text{NO}_3)_2/\text{NF}$.

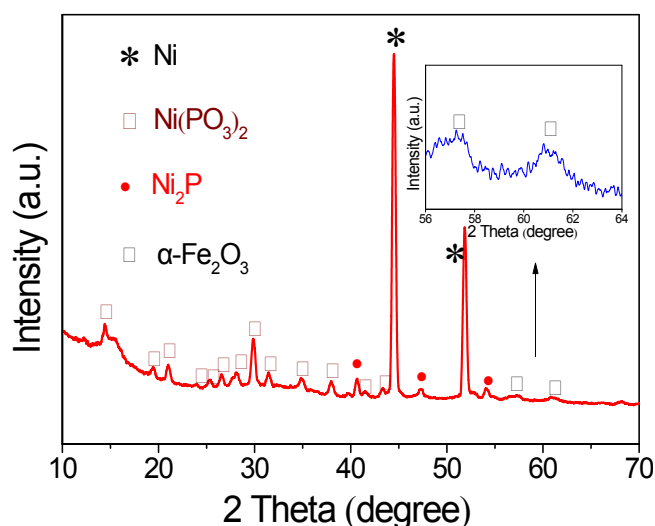


Figure S4. XRD pattern of $\text{Fe}_2\text{O}_3@\text{Ni}_2\text{P}/\text{Ni}(\text{PO}_3)_2/\text{NF}$, inset: the enlarged XRD pattern of $\text{Fe}_2\text{O}_3@\text{Ni}_2\text{P}/\text{Ni}(\text{PO}_3)_2/\text{NF}$.

X-ray diffraction (XRD) pattern of the 3D $\text{Fe}_2\text{O}_3@\text{Ni}_2\text{P}/\text{Ni}(\text{PO}_3)_2/\text{NF}$ hybrid confirms the coexistence of Fe_2O_3 , Ni_2P , and $\text{Ni}(\text{PO}_3)_2$. Besides two conspicuous peaks of metallic Ni, the main XRD peaks are exactly associated to those of the Fe_2O_3 , Ni_2P , and $\text{Ni}(\text{PO}_3)_2$ (JCPDS 33-0664, 74-1385, and 28-0708), in which two weak peaks centered at 57.4 and 61.5° are related to the (0 1 8) and (1 1 4) planes of metallic Fe_2O_3 , and three strong peaks centered at 40.6 , 47.2 and 54.2° are related to the (1 1 1), (2 1 0) and (3 0 0) planes of Ni_2P , respectively. The remaining other XRD peaks are assigned to the $\text{Ni}(\text{PO}_3)_2$.

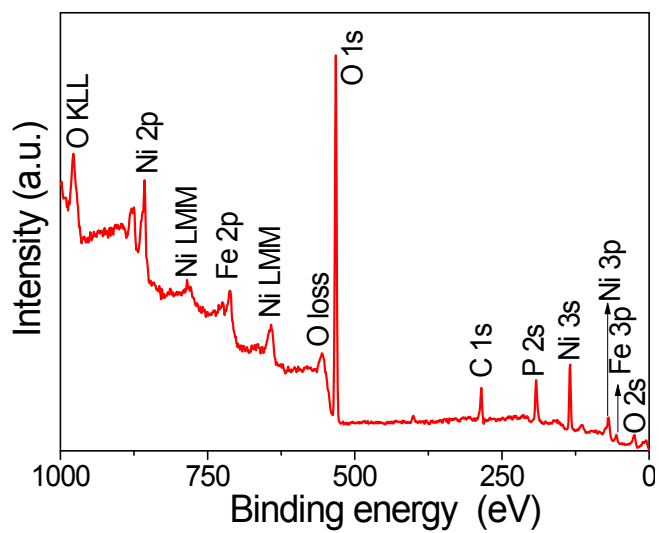


Figure S5. XPS survey spectrum of $\text{Fe}_2\text{O}_3@\text{Ni}_2\text{P}/\text{Ni}(\text{PO}_3)_2/\text{NF}$ hybrid.

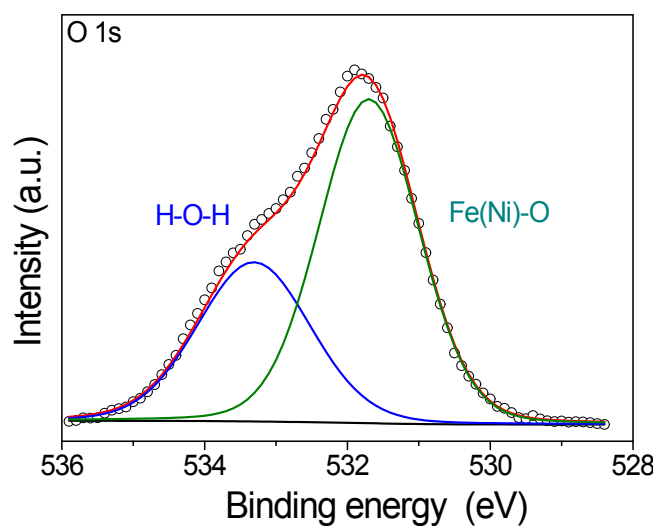


Figure S6. High resolution O 1s XPS spectra of Fe₂O₃@Ni₂P/Ni(NO₃)₂/NF.

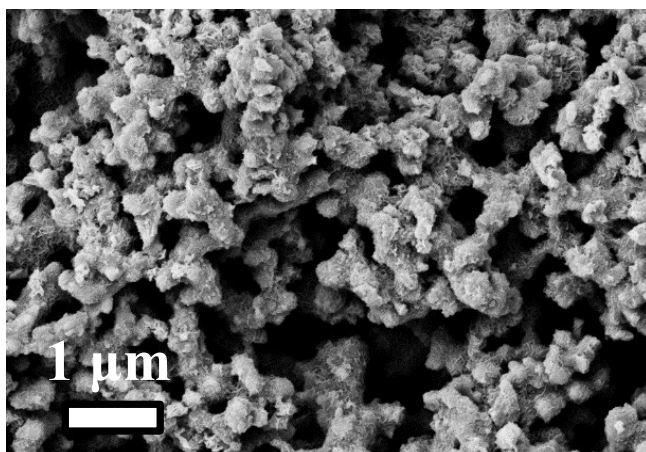


Figure S7. FESEM image of $\text{Fe}_2\text{O}_3@\text{Ni}_2\text{P}/\text{Ni}(\text{PO}_3)_2/\text{NF}$ hybrid after OER process.

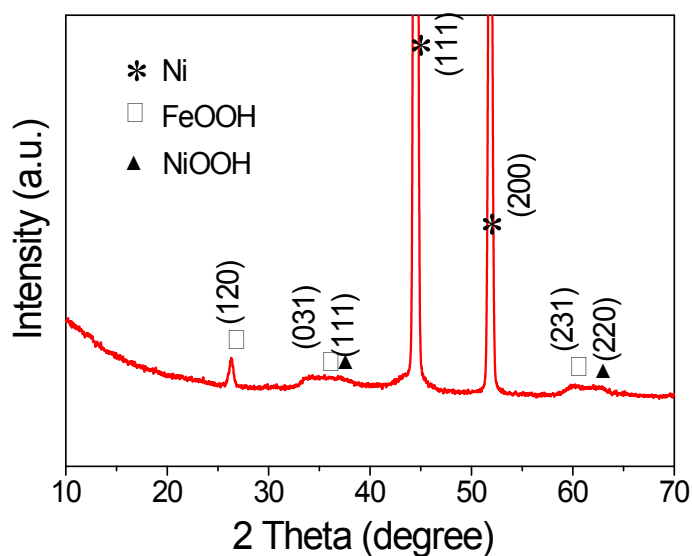


Figure S8. XRD pattern of $\text{Fe}_2\text{O}_3@\text{Ni}_2\text{P}/\text{Ni}(\text{NO}_3)_2/\text{NF}$ hybrid after OER process.

The XRD pattern of $\text{Fe}_2\text{O}_3@\text{Ni}_2\text{P}/\text{Ni}(\text{NO}_3)_2/\text{NF}$ hybrid after OER stability test displays that the species of $\text{Fe}_2\text{O}_3@\text{Ni}_2\text{P}/\text{Ni}(\text{NO}_3)_2/\text{NF}$ was changed from Fe_2O_3 , Ni_2P and $\text{Ni}(\text{NO}_3)_2$ to the final FeOOH and NiOOH phases. The results revealed that the transformation of components in $\text{Fe}_2\text{O}_3@\text{Ni}_2\text{P}/\text{Ni}(\text{NO}_3)_2/\text{NF}$ hybrid was occurred during OER process, in which the Fe_2O_3 and $\text{Ni}_2\text{P}/\text{Ni}(\text{NO}_3)_2$ species could be converted into active NiOOH and FeOOH species under alkaline condition, respectively, acting as the active phases during OER process and leading to the high performance of $\text{Fe}_2\text{O}_3@\text{Ni}_2\text{P}/\text{Ni}(\text{NO}_3)_2/\text{NF}$.

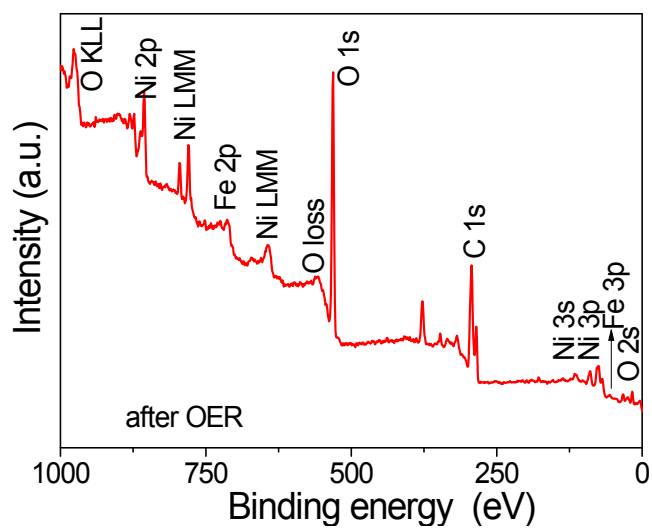


Figure S9. XPS survey spectrum of Fe₂O₃@Ni₂P/Ni(PO₃)₂/NF hybrid after OER process.

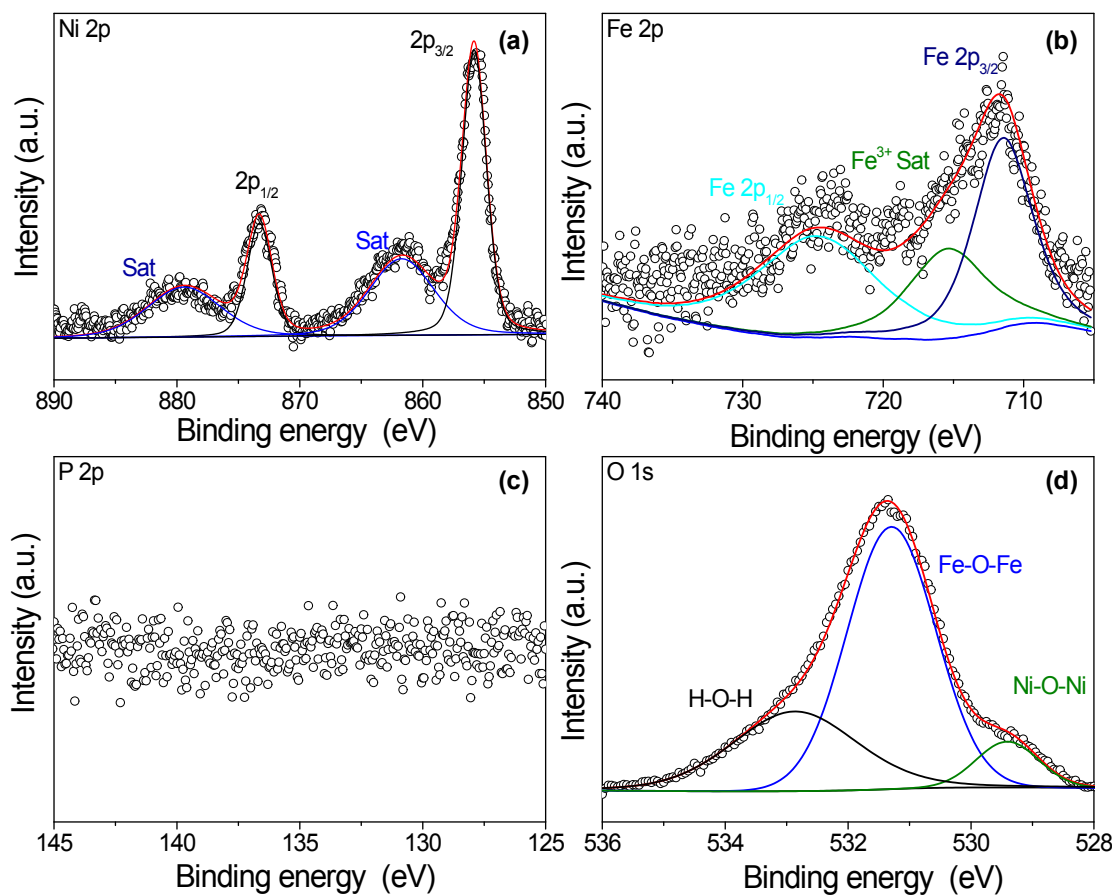


Figure S10. (a) High-resolution Ni 2p, (b) Fe 2p, (c) P 2p, and (d) O 1s XPS spectra of $Fe_2O_3@Ni_2P/Ni(PO_3)_2/NF$ after OER process.

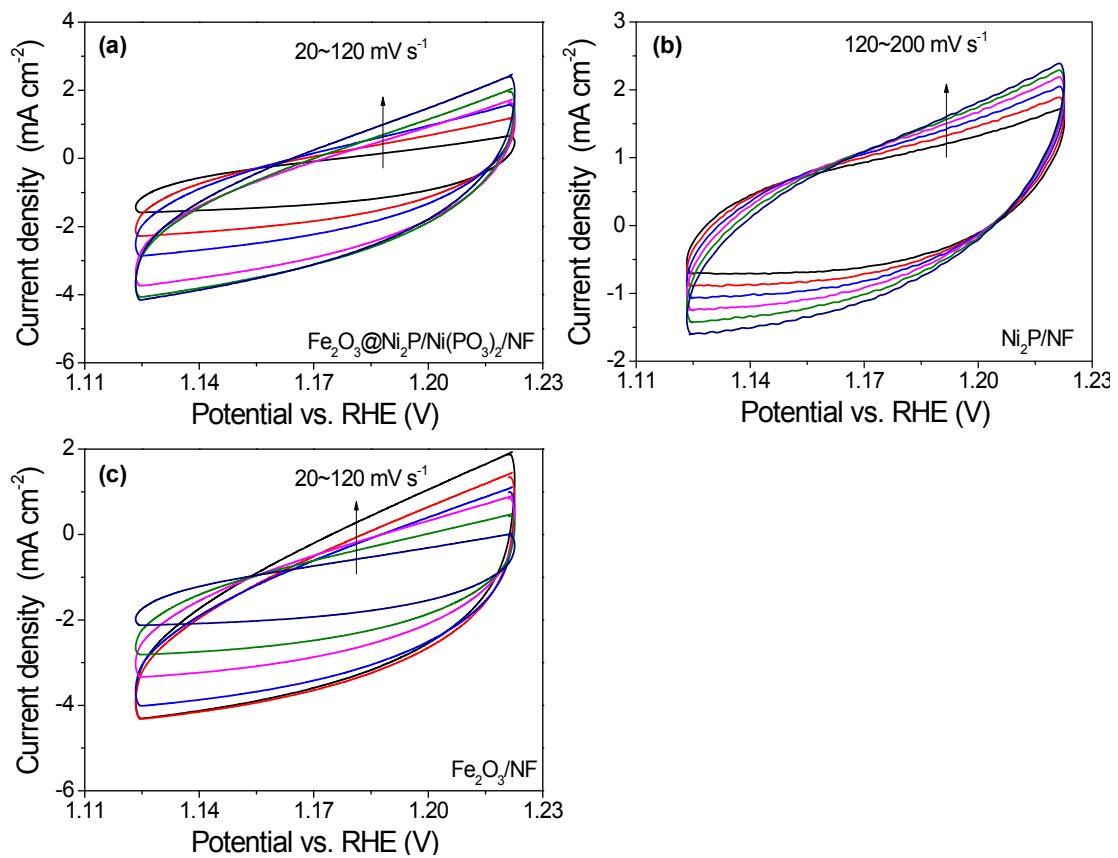


Figure S11. ECSAs of (a) $\text{Fe}_2\text{O}_3@\text{Ni}_2\text{P}/\text{Ni}(\text{PO}_3)_2/\text{NF}$, (b) $\text{Ni}_2\text{P}/\text{NF}$, and (c) $\text{Fe}_2\text{O}_3/\text{NF}$.

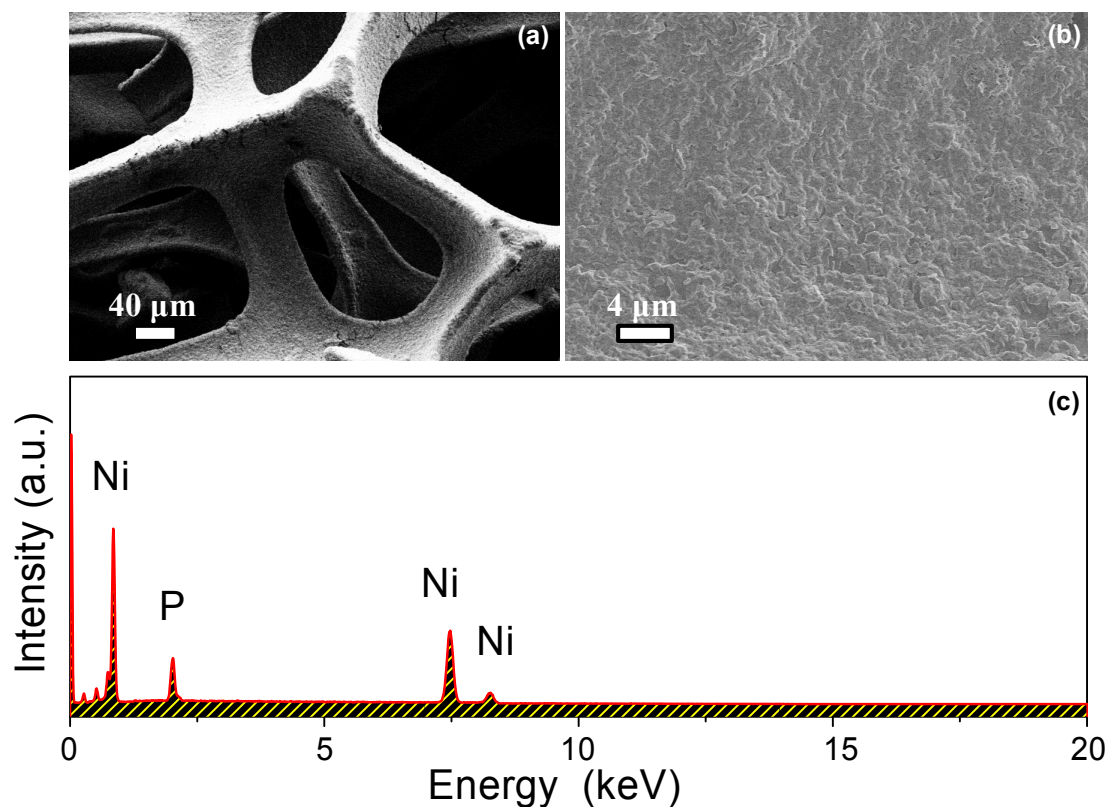


Figure S12. (a-b) FESEM images of $\text{Ni}_2\text{P}/\text{NF}$, and (c) EDX spectrum of the $\text{Ni}_2\text{P}/\text{NF}$.

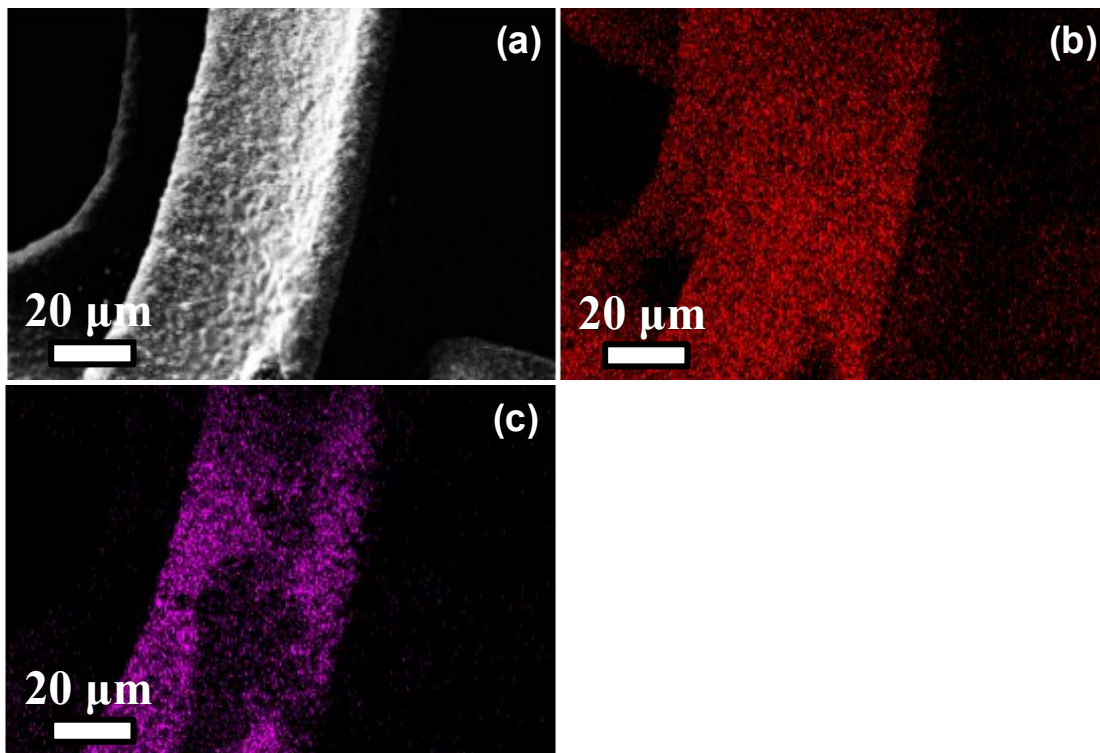


Figure S13. (a) FESEM image of Ni₂P/NF, and (b-c) elemental mappings of Ni₂P/NF.

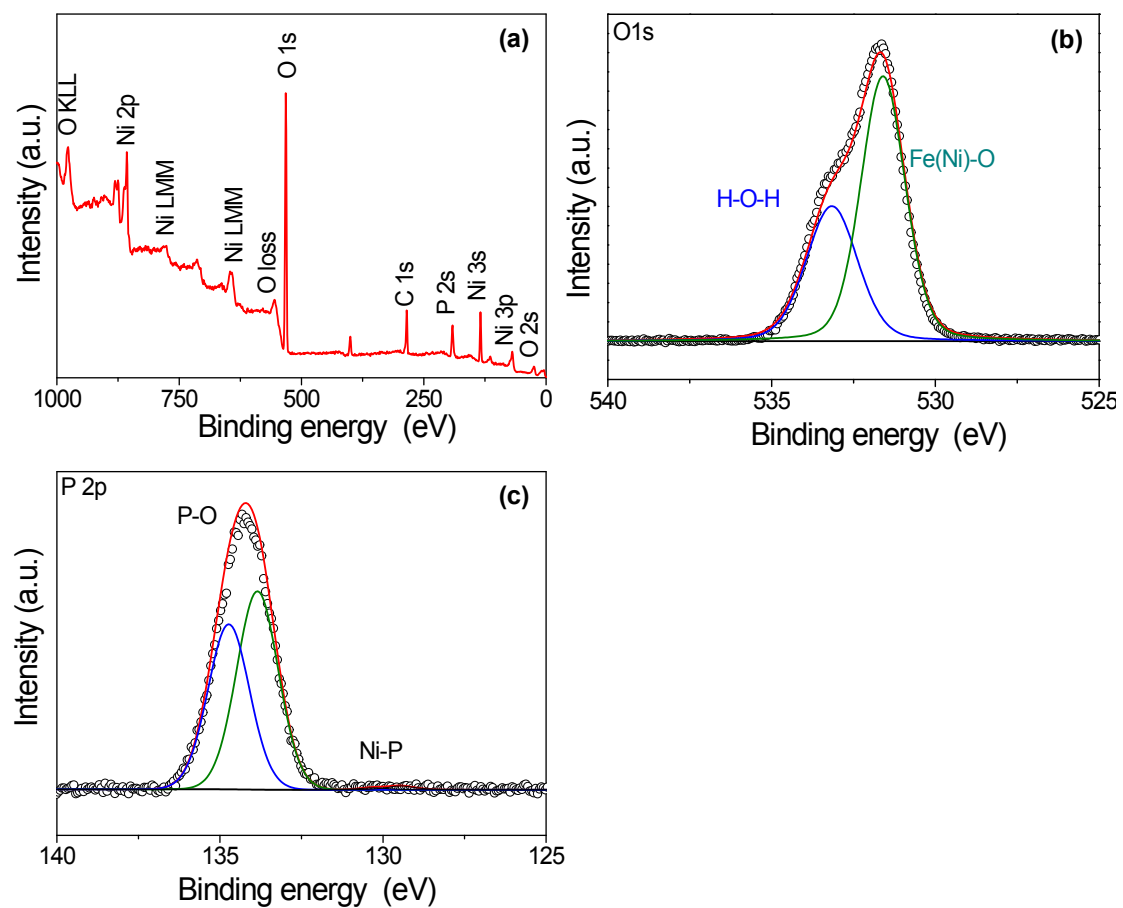


Figure S14. (a) The XPS survey spectrum of Ni_2P ; high-resolution (b) O 1s and (c) P 2p XPS spectra of Ni_2P .

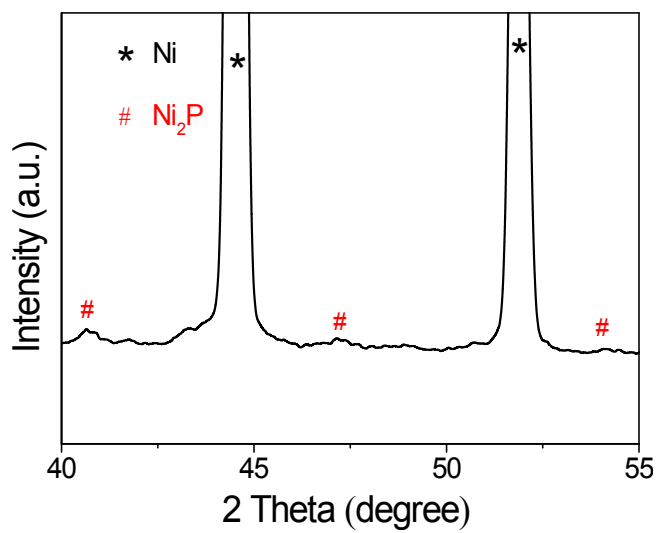


Figure S15. XRD pattern of Ni₂P/NF.

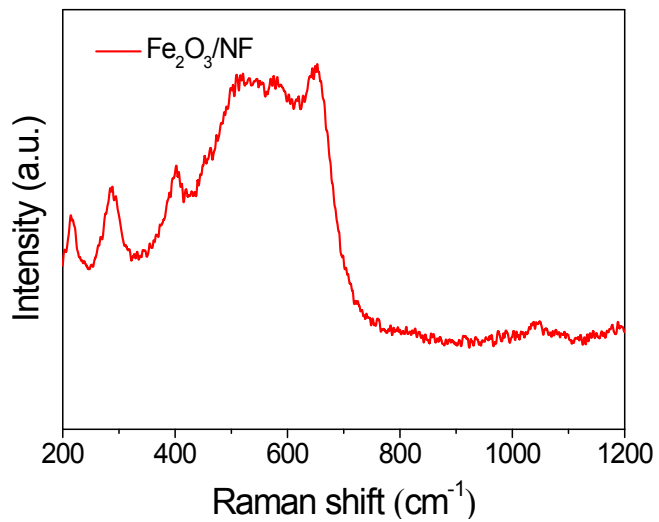


Figure S16. Raman spectrum of Fe₂O₃/NF.

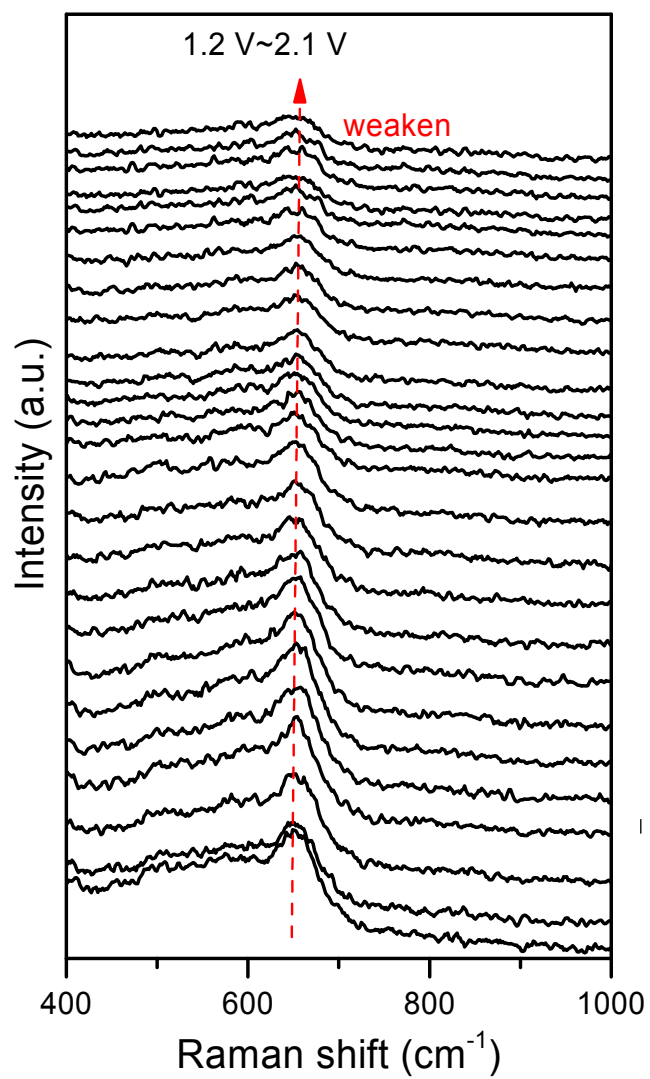


Figure S17. In situ Raman spectra of Fe₂O₃/NF during the OER process.

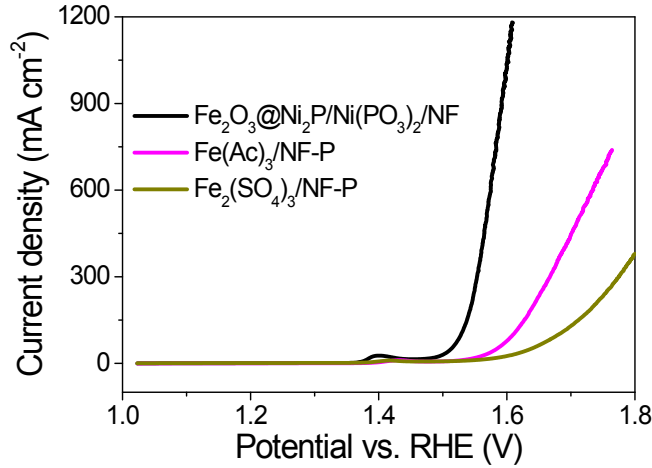
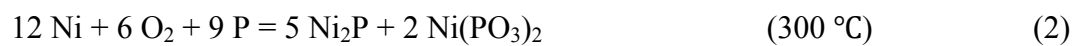
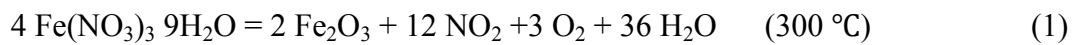


Figure S18. Polarization curves of Fe₂O₃@Ni₂P/Ni(PO₃)₂/NF, Fe(Ac)₃/NF-P, and Fe₂(SO₄)₃/NF-P.

Formation mechanism.

A possible mechanism toward the growth of 3D Fe₂O₃@Ni₂P/Ni(PO₃)₂/NF hybrid is unveiled by combining above characterization results. It is based on two specific chemical reactions which should take place concurrently in this vacuum environment as below:



First, the NF substrate soaked with Fe(NO₃)₃ solution, and red phosphorus powder were heated in a vacuum quartz tube at 300 °C, in which the heat drives the Fe(NO₃)₃ · 9 H₂O to form the Fe₂O₃, O₂, NO₂, and H₂O (equation (1)).¹ Then, Ni₂P and Ni(PO₃)₂ can be obtained at 300 °C via an ingenious disproportionation reaction based on equation (2), which is quite unusual compared with the situation in those previous reports, in which either Ni(PO₃)₂ or Ni₂P was generated.^{2,3}

The existence of O₂ was required for the formation of Ni₂P and Ni(PO₃)₂. To clarify

this point, the thermal phosphorization strategy was further extended to synthesize the control samples by changing anion of iron solution (anion = NO_3^- , Ac^- , SO_4^{2-}) with the same experimental conditions (Figure S18). Among these synthesized samples ($\text{Fe}_2(\text{SO}_4)_3/\text{NF-P}$, $\text{Fe}(\text{Ac})_3/\text{NF-P}$, and $\text{Fe}_2\text{O}_3@\text{Ni}_2\text{P}/\text{Ni}(\text{PO}_3)_2/\text{NF}$), the 3D $\text{Fe}_2\text{O}_3@\text{Ni}_2\text{P}/\text{Ni}(\text{PO}_3)_2/\text{NF}$ hybrid exhibits the best OER performance, which can be attributed to the formation of both Ni_2P and $\text{Ni}(\text{PO}_3)_2$.

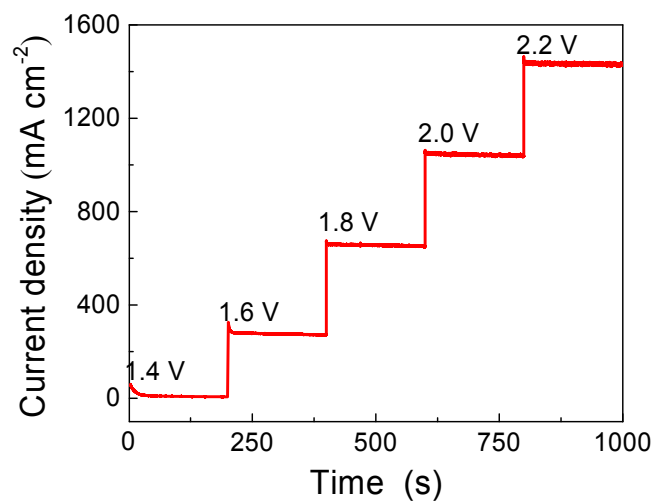


Figure S19. The multi-potential steps curve for Fe₂O₃@Ni₂P/Ni(PO₃)₂/NF.

Table S1. OER activities of representative benchmark electrocatalysts in alkaline solution in terms of the potential to achieve a current density of 100, 500, and 1000 mA cm⁻².

Material	Electrolyte	Substrate	Tafel slope (mV dec ⁻¹)	Potential vs. RHE(V)		
				100 mA cm ⁻²	500 mA cm ⁻²	1000 mA cm ⁻²
Fe₂O₃@Ni₂P/Ni(PO₃)₂ (in this work)	1.0 M KOH	NF	48.2	1.53	1.57	1.60
Fe(PO ₃) ₂ /Ni ₂ P ⁴	1 M KOH	NF	51.9	1.45	1.50	1.52*
FeP/Ni ₂ P ⁵	1 M KOH	NF	22.7	1.60	1.72	1.78
Ni ₁₁ (HPO ₃) ₈ (OH) ₆ ⁶	1 M KOH	NF	91	1.59	1.76	
(Fe _x Ni _{1-x}) ₂ P ⁷	1 M KOH	NF	66	1.44	1.48	
M-Ni ₂ P/Fe ₂ P-O ⁸	1 M KOH	NF	42.7	1.48	-	-
Co-S ₅₈ -P ₄₂ ⁹	1 M KOH	anode slurry	48	1.58	-	-
FeCoNiP ¹⁰	1 M KOH	GC	70	1.50	-	-
CoNiP ¹⁰	1 M KOH	GC	78	1.55	-	-
FeCoP ¹⁰	1 M KOH	GC	86	1.58	-	-
FeNiP ¹⁰	1 M KOH	GC	91	1.61	-	-
CoP ¹⁰	1 M KOH	GC	99	1.63		

NiP ¹⁰	1 M KOH	GC	107	1.64	-	-
FeP ¹⁰	1 M KOH	GC	131	1.65		
CoP ¹¹	1 M KOH	NW	78	1.53		
Ni ₂ P ₂ S ₆ ¹²	1 M KOH	NF	83.2	1.55	-	-
	1 M KOH	CFP	40.3	1.53	-	-
P-Co ₃ O ₄ ¹³	1MKOH	NF	110		1.57*	-

Reference

1. X. K. Wan, X. Q. Zou, H. X. Shi and D. H. Wang, *Journal of Zhejiang University-Science A*, 2007, **8**, 707-711.
2. J. Xu, J. P. S. Sousa, N. E. Mordvinova, J. D. Costa, D. Y. Petrovykh, K. Kovnir, O. I. Lebedev and Y. V. Kolen'ko, *ACS Catal.*, 2018, **8**, 2595-2600.
3. Q. Liu, C. Y. Chen, J. J. Zheng, L. Wang, Z. Yang and W. Yang, *J. Am. Chem. Soc.*, 2017, **5**, 1421-1427.
4. H. Zhou, F. Yu, J. Sun, R. He, S. Chen, C. W. Chu and Z. Ren, *Proc. Natl. Acad. Sci. U. S. A.*, 2017, **114**, 5607-5611.
5. F. Yu, H. Zhou, Y. Huang, J. Sun, F. Qin, J. Bao, W. A. Goddard, 3rd, S. Chen and Z. Ren, *Nat. Commun.*, 2018, **9**, 2551.
6. W. M. Prashanth, P. Chakadola, L. Stefan, B.-B. Florian, W. Carsten, S. Michael, D. Xiaohui, D. Holger and D. Matthias, *Energy Environ. Sci.*, 2018, **11**, 1287-1298.
7. B. Zhang, Y. H. Lui, H. Ni and S. Hu, *Nano Energy*, 2017, **38**, 553-560.
8. P. F. Liu, X. Li, S. Yang, M. Y. Zu, P. R. Liu, B. Zhang, L. R. Zheng, H. J. Zhao and H. G. Yang, *ACS Energy Lett.*, 2017, **2**, 2257-2263.
9. Z. Dai, H. Geng, J. Wang, Y. Luo, B. Li, Y. Zong, J. Yang, Y. Guo, Y. Zheng, X. Wang and Q. Yan, *ACS Nano*, 2017, **11**, 11031-11040.
10. J. Xu, J. Li, D. Xiong, B. Zhang, Y. Liu, K. H. Wu, I. Amorim, W. Li and L. Liu, *Chem Sci*, 2018, **9**, 3470-3476.
11. W. Li, X. Gao, D. Xiong, F. Xia, J. Liu, W. G. Song, J. Xu, S. M. Thalluri, M. F. Cerqueira, X. Fu and L. Liu, *Chem Sci*, 2017, **8**, 2952-2958.
12. X. Y. Zhang, S. Zhang, J. Li and E. K. Wang, *J. Am. Chem. Soc.*, 2017, **5**, 22131-22136.
13. Z. Wang, H. Liu, R. Ge, X. Ren, J. Ren, D. Yang, L. Zhang and X. Sun, *ACS Catal.*, 2018, **8**, 2236-2241.